Catalysis Science & Technology

Accepted Manuscript

ROYAL SOCIETY OF CHEMISTRY

www.rsc.org/catalysis

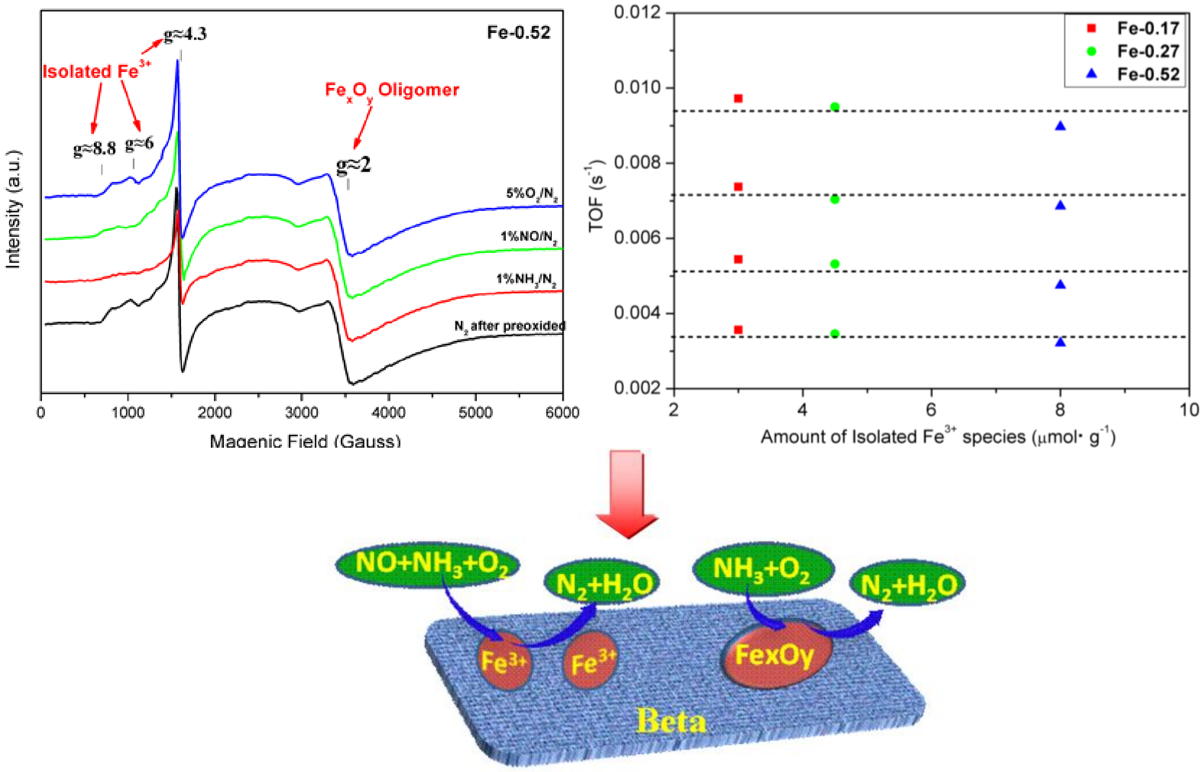

Fe-0.52
Isolated Fe^{3+}
g≈4.3
g≈8.8
g≈6
Fe_xO_y Oligomer
g≈2
5%O_2/N_2
1%NO/N_2
1%NH_3/N_2
N_2 after preoxided
Intensity (a.u.)
Magenic Field (Gauss)
0
1000
2000
3000
4000
5000
6000
TOF (s^{-1})
0.012
0.010
0.008
0.006
0.004
0.002
2
4
6
8
10
Amount of Isolated Fe^{3+} species (μmol· g^{-1})
Fe-0.17
Fe-0.27
Fe-0.52
NO+NH_3+O_2
N_2+H_2O
NH_3+O_2
N_2+H_2O
Fe^{3+}
Fe^{3+}
FexOy
Beta

Cite this: DOI: 10.1039/c0xx00000x

www.rsc.org/xxxxxx

ARTICLE TYPE

The role of various iron species in Fe-Beta catalysts with low iron loadings for NH_3-SCR

Haiyan Liu,[a,c] Tie Yu,[a] Shikuan Fan,[a] Jun Wang[a] and Meiqing Shen*[a, b]

Received (in XXX, XXX) Xth XXXXXXXXX 20XX, Accepted Xth XXXXXXXXX 20XX
DOI: 10.1039/b000000x

A series of Fe-Beta catalysts, containing 0.17-0.52 wt% Fe, were prepared by liquid ion-exchange method to study the influence of various iron species on the NH_3-SCR activity. A combination of UV-vis and EPR techniques was applied to identify and quantify the iron species. The spectroscopic studies showed that the iron were almost only isolated Fe^{3+} as Fe content was less than or equal to 0.17 wt%. At higher Fe content (0.27-0.52 wt% Fe), small oligomers coexisted with isolated Fe^{3+} species. Furthermore, the quantitative analysis indicated that the percentage of tetrahedral Fe^{3+} isolates decreased, while the percentage of octahedral Fe^{3+} isolates increased with the increment of iron loading. *In situ* EPR results suggested that isolated Fe^{3+} performed excellent activity for NH_3-SCR; moreover, isolated Fe^{3+} sites in distorted tetrahedral (g≈6) and octahedral (g≈8.8) environment performed better redox ability than tetrahedral Fe^{3+} (g≈4.3). The SCR TOF values proved that isolated Fe^{3+} sites both in tetrahedral and octahedral coordination were the active sites for NH_3-SCR reaction. In addition, the NH_3 oxidation TOF results indicated that oligomers were the active sites for NH_3 oxidation over Fe-Beta catalysts and the contribution of diverse clustered oligomers was unequal.

1 Introduction

Selective catalytic reduction of NO_x by ammonia (NH_3-SCR) is an effective and efficient technology to reduce NO_x emission from lean-burn engines[1]. Many researchers have focused on Fe-based zeolite, such as Fe-ZSM-5, Fe-MOR, Fe-MFI and Fe-Beta [2-6]. Among these zeolites, Fe-Beta has been drawn great attention due to its remarkable catalytic activity and hydrothermal stability during SCR process.

In recent years, several groups[6-17] have made extensive studies on Fe-Beta for NH_3-SCR. The researches[7-9] found that a variety of Fe species, including isolated Fe^{3+}, Fe_xO_y oligomers of varying nuclearity and Fe_2O_3 particles, coexisted in Fe-Beta. And the distribution of Fe species was influenced by the iron content and synthesis methods. Frey et al.[10] synthesized Fe-Beta by incipient wetness impregnation (IWI) and isomorphous substitution (IS). They found that the IWI sample was dominated by both the isolated Fe^{3+} and the oxide species, while the IS sample mainly contained higher coordinated iron. Høj et al.[8] and Ma et al.[9] prepared Fe-Beta catalysts with different iron loadings by incipient wetness impregnation and aqueous ion exchange. Their results showed that the sample with low iron loadings was mainly isolated Fe^{3+} species. But the quantitative analysis of various iron species was seldom made over Fe-Beta catalyst. In addition, the active site for NH_3-SCR over Fe-Beta was also studied. Recently, Balle et al.[11] found isolated Fe oxo structures revealed higher performance than oligomers and particles. Doronkin et al.[7] prepared Fe-Beta by Ca-form zeolite and suggested isolated Fe^{3+} in cationic positions was the active sites for NH_3-SCR. Høj et al.[8] studied the relationship between monomers and NO conversion and indicated monomers were active in the SCR reaction. Maier et al.[15] and Kim et al.[16] characterized the iron species under NH_3-SCR conditions. They found that the bridging Fe-O-Fe dimmers formed and were active in NH_3-SCR reaction. However, so far, there is still controversy over the structure of the active sites for NH_3-SCR over Fe-Beta. Furthermore, the research on the relationship between the number of active sites and the SCR reaction rates are seldom reported.

In this work, the purpose is to identify and quantify iron species in Fe-Beta catalysts and illustrate the connection between the quantitative iron species and SCR reaction rate, thereby clarifying their role in NH_3-SCR reaction. We prepared three Fe-Beta samples by the same procedure and controlled the iron loading due to the multiformity of the iron species. UV-Vis and EPR spectroscopy were applied to characterize different iron species in Fe-Beta catalysts. The performance of NH_3-SCR and NH_3 oxidation over Fe-Beta catalysts was also evaluated. *In situ* EPR experiments were tested to investigate the variation of iron species and their role in NH_3-SCR reaction. In addition, kinetics experiments were conducted to find the correlation between the number of active sites and the SCR reaction rates.

2 Experimental

2.1 Catalysts preparation

A series of Fe-beta catalysts with low iron loadings were prepared by liquid ion-exchange method over Na-beta supports (SiO_2/Al_2O_3=30, supplied by Qichuang Chemical Technology Company). Firstly, 10 g Na- beta was mixed with100 mL 27% NH_4NO_3 (99% NH_4NO_3, Tianjin Kewei Chemical Co., China) solution with constant stirring at 80 ℃ for 4 h. Then, the mixture was filtered and washed with deionized water. The obtained solids were subsequently dried at 120 ℃ for 12 h and calcined at 550 ℃ for 4 h in airflow to obtain H- beta. The Fe- beta catalysts were prepared by mixing 10 g H- beta with 200 mL $FeCl_2$ (98%, $FeCl_2.4H_2O$, Tianjin Kewei Chemical Co., China) solution, and the detailed $FeCl_2$ concentrations are listed in Table 1. The slurry was vigorously mixed at 70 ℃ for 12 h and the pH value was kept at 3.0 ~ 3.5. Then, the solid was filtered and washed with deionized water until no chloridion was observed (detected by $AgNO_3$ solution). Finally, the washed sample was dried and further calcined under the same condition as H-Beta. The details of the samples are listed in Table1.

Table 1 Description of Fe-Beta catalysts and concentration of ion-exchange solution

Samples	Fe Content *[a] (wt%)	Al Content *[a] (wt%)	Iron exchange extent (%) *[b]	Concentration of $FeCl_2$ (mol L^{-1})
Fe-0.17	0.17	1.49	16.5	0.001
Fe-0.27	0.27	1.56	24.9	0.002
Fe-0.52	0.52	1.63	46.1	0.005

*[a]: Fe and Al contents were analyzed by ICP.
*[b]: Calculated by 3 ×(number of iron ions)/ (number of aluminum ions).

2.2 Catalytic activity measurement

Activity measurement was carried out in a quartz reactor (20 mm inner diameter). The gas concentrations were analyzed by Fourier Transform Infrared (FTIR) spectrometer (MKS-2030) equipped with a 5.11 m gas cell. The 250 mg catalysts (powder 60-80 mesh) mixed with quartz sands were used for NH_3-SCR and NH_3 oxidation measurements (GHSV=56,000 h^{-1}).The gas mixture consisted of 500 ppm NO, 500 ppm NH_3, 5% O_2 balanced with N_2 for the NH_3-SCR reaction and 500 ppm NH_3, 5% O_2 balanced with N_2 for the NH_3 oxidation reaction. 5% H_2O and 8% CO_2 were present all the time. All experiments were performed at atmospheric pressure and under steady-state conditions at a pre-determined temperature. Prior to the activity evaluation, the catalysts were pretreated at 550 ℃ for 30 min in 5% O_2/N_2. The catalytic activities were measured from 150 ℃ to 600 ℃. The NO_x and NH_3 conversions were calculated by Eq. (1) and (2) which based on the inlet and outlet gas concentrations.

$$NO_x\ \text{Conversion} = \frac{(NO + NO_2)_{inlet} - (NO + NO_2 + 2N_2O)_{outlet}}{(NO + NO_2)_{inlet}} \times 100\% \quad (1)$$

$$NH_3\ \text{Conversion} = \frac{NH_{3\ inlet} - NH_{3\ outlet}}{NH_{3\ inlet}} \times 100\% \quad (2)$$

2.3 Kinetic measurements

The NH_3-SCR kinetic experiments of Fe-Beta catalysts were obtained in a thin quartz tube. 50 mg catalysts mixed with quartz sand in a quantity ratio of 1:3 were placed in the reactor. The samples with particles of 60-80 mesh and the gas hourly space velocity (GHSV) of 420,000 h^{-1} were selected to rule out the mass transfer diffusions (details with Fig. S1 and S2 are included in the supporting information). The samples were pre-treated in 5% O_2/N_2 at 550 ℃ before the kinetic experiments. The reaction gas consisted of 500 ppm NO, 500 ppm NH_3, 5% O_2, 5% H_2O and 8% CO_2 with N_2 as the balance. The kinetic steady-state measurements were obtained from 220 ℃ to 280 ℃ at 20 ℃ intervals and each temperature stable for at least 1.5 h.

The NH_3 Oxidation kinetic experiments were conducted under the same condition with NH_3-SCR. The results in Fig.S3 and Fig.S4 (details in supplement information) indicate that the NH_3 oxidation rates under that condition are truly kinetically controlled and not mass transfer limited. The inlets consisted of 500 ppm NH_3, 5% O_2, 5% H_2O and 8% CO_2 with N_2 as the balance. The kinetic steady-state measurements were obtained from 460 °C to 520 °C at 20 ℃ intervals and each temperature stable for at least 1.5 h.

2.4 Catalysts characterization

UV-vis-DRS (diffuse reflectance spectroscopy) measurements were carried out at room temperature on a Shimadzu 3600 UV–Visible spectrophotometer equipped with a diffuse reflectance accessory. Spectra were presented in reflectance mode and converted into the Kubelka–Munk function being defined as $F(R) = (1- R)^2/2R$. To reduce light absorption, samples were diluted by $BaSO_4$ (dried at 120 ℃ for 12h) in a ratio of 1:10. The samples were pretreated in 5% O_2/N_2 at 550 ℃ for 30 min to avoid overestimation of the amount of isolated Fe^{3+} species[18]. Deconvolution of UV–Vis spectra to peaks was conducted using Origin 8.0 software. The various iron species were quantified relative to each other by the area ratios of the corresponding sub-bands.

X-band (ν= 9.78 GHz) EPR spectra were recorded on a Bruker model A320 instrument, equipped with a commercial variable temperature control unit. All EPR measurements were performed in a homemade three-sleeve quartz EPR reactor. The reactor connected to a gas-dosing system was implemented in a rectangular ER 4102st cavity. Before the measurements, the samples (77 mg) were pretreated in 5% O_2/N_2 at 550 ℃ for 30 min, then cooled down to room temperature in N_2. The EPR signals were registered at room temperature, microwave power 6.4 mW and modulation amplitude 3.0 G in the field range of 500-6,500 G. The standard sample DPPH (g=2.0036) was used for calibration of the instrument error before every measurement.

In situ EPR measurement was tested at 250 ℃ and the EPR spectra was recorded under steady-state condition. The catalysts were exposed to the following sequence of experimental steps[13, 19]: (1) pretreated in 5% O_2/N_2 (25 mL min^{-1}) for 30 min, then treated in N_2 for 1 h; (2) treated in 0.1% NH_3/ N_2 (25 mL min^{-1}) for 1 h; (3) treated in 0.1% NO/ N_2 (25 mL min^{-1}) for 1 h; (4) re-oxidized in 5% O_2/N_2 (25 mL min^{-1}) at 250 ℃ for 1 h.

3 Results and Discussion

3.1 NH_3-SCR catalytic activity and NH_3 oxidation activity

The NH_3-SCR catalytic activity over various catalysts is shown in Fig.1. Fig.1a indicates the NO_x conversion as a function of temperature over H-Beta and Fe-Beta catalysts. Compared with Fe-Beta catalysts, the activity of H-Beta is much lower during the whole testing temperature, indicating that the addition of iron to H-Beta significantly improves the NH_3-SCR activity. And the catalytic activity of Fe-Beta increases with the increment of iron loading. In addition, the NO_x conversion slightly declines at high temperature, especially for Fe-0.52 sample the NO_x conversion reduces nearly 10% from 500 to 600 ℃. Fig. 1b shows the N_2O concentration formed during the NH_3-SCR process. The maximum N_2O concentration reached 18ppm at 350 ℃ over H-Beta. All Fe-Beta catalysts produce little amounts of by-product N_2O, which is less than 5 ppm for the entire range of testing temperatures, indicating excellent N_2 selectivity. Fig. 1c shows the NH_3 conversion as a function of temperature during the NH_3-SCR process. Generally, the NH_3 conversion is a little higher than the NO_x conversion, particularly at high temperature.

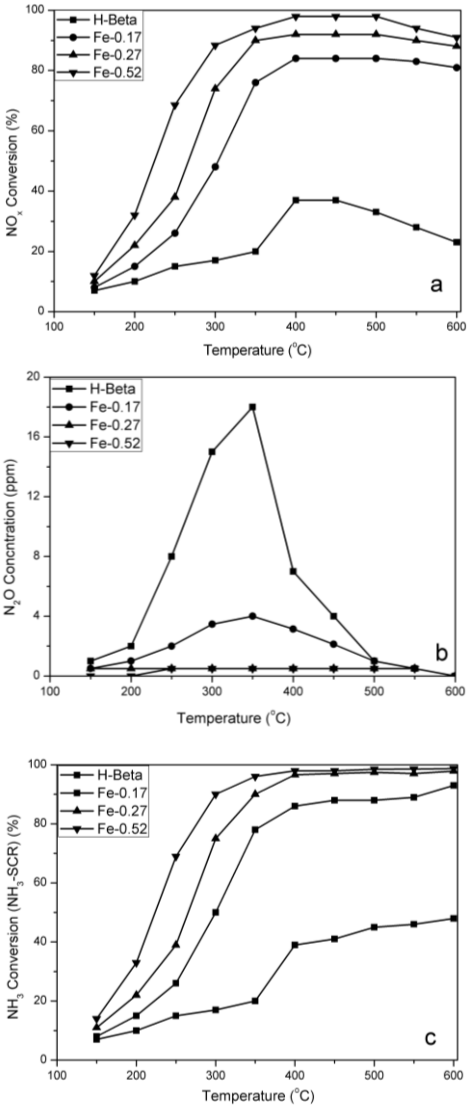

Fig.1. Catalytic activity for NH_3-SCR on different catalysts; reaction conditions: 500 ppm NO, 500 ppmNH_3, 5% O_2, 8% CO_2, 5% H_2O balanced with N_2; flow rate: 1L min^{-1}; GHSV: 56,000 h^{-1}. a) NO_x conversion; b) N_2O concentration; c) NH_3 conversion.

Compared to the NH_3-SCR activity, the activity of NH_3 oxidation was also investigated over different samples (Fig. 2). Comparing the excellent NH_3-SCR activity, NH_3 oxidation presents inferior performance over Fe-Beta. The pattern in Fig. 2 suggests that the NH_3 conversion over Fe-Beta is almost the same below 400 ℃ and improves with the increment of iron loading above 400 ℃. Fe-0.52 sample exhibits the maximum NH_3 conversion for 67% at 600 °C. H-Beta indicates a similar NH_3 oxidation activity with Fe-0.17 sample. Considering that the different kinds of iron species maybe exist in Fe-Beta due to the diverse iron loading, it seems that the various iron species in Fe-Beta catalysts perform diverse catalytic ability for NH_3-SCR and NH_3 oxidation, which will be discussed later.

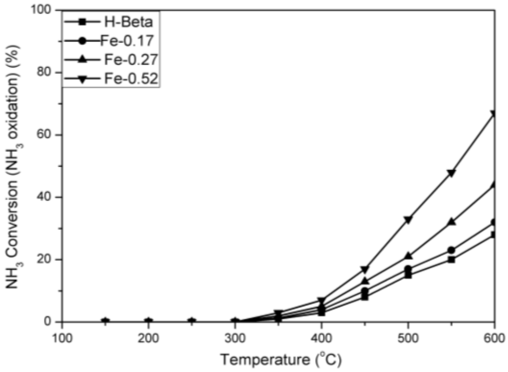

Fig.2. NH_3 oxidation conversions as a function of reaction temperature; reaction conditions: 500 ppmNH_3, 5% O_2, 8% CO_2, 5% H_2O balanced with N_2; flow rate: 1L min^{-1}; GHSV: 56,000 h^{-1}.

3.2 Characterization of iron species

UV-vis results

UV-vis spectroscopy is used to characterize the nature and distribution of various iron species. Fig. 3 shows the UV-vis spectra of Fe-Beta with deconvolution into the lowest number of sub-bands to help assignment various iron species. In this work, the bands at ~220 nm and ~275 nm are ascribed to isolated Fe^{3+} species in tetrahedral and octahedral coordination, respectively; the bands between 300 nm and 400 nm are ascribed to octahedral Fe^{3+} in small oligomeric Fe_xO_y clusters, and the bands above 400 nm are ascribed to large Fe_2O_3 particles located at the external surface of the zeolite crystal[20-22]. Table 2 summarizes the amount of various iron species derived from the intensity of the sub-bands and the relative percentage, and the total iron contents in the samples.

In Fig. 3, all of the spectra exhibit two bands in the UV region at ~220 nm and ~275 nm. Furthermore, the peaks reveal red shift and the intensity of peaks rises with the increment of iron loading. According to the results in Table 2, almost all irons in Fe-0.17 sample are isolated Fe^{3+} and more than 90% of irons in Fe-0.27 sample are isolated Fe^{3+}, while the percentage of isolated Fe^{3+} reduces to 86% in Fe-0.52 sample. Furthermore, the percentage of isolated Fe^{3+} decrease, while the percentage of oligomic Fe_xO_y clusters increase with the increment of iron loading. However, due to the increment of iron content, the amount of various iron species increases (see Table 2). In addition, the amount of small oligomeric Fe_xO_y clusters increases as the iron content increases. It is worth note that there is no Fe_2O_3 particles observed in Fe-0.52 sample (ion exchange degree = 46.1 %). The similar result was discussed by Zhilinskaya et al.[23] and Mauvezin et al.[24]. The proportion of oligomer species increased when the ion exchange extent was above 24 %. And this iron species prevail until the ion exchange level to 100 %. Fe_2O_3 particles were only present when the iron exchange level exceeded 100 %.

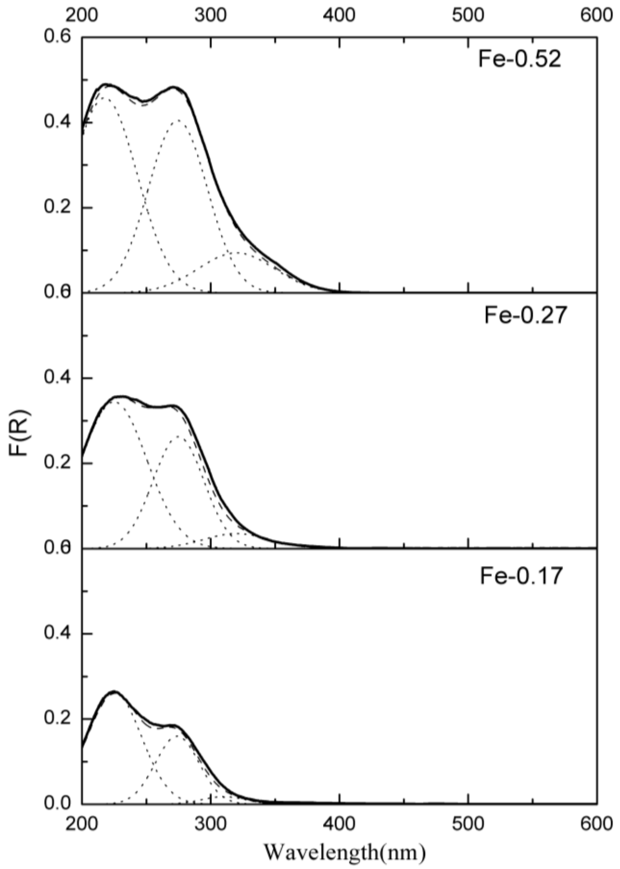

Fig.3. UV-vis spectra of Fe-beta samples recorded at room temperature after pre-oxidized at 550 ºC for 30 min including sub-bands as derived by deconvolution. Experimental spectra: thick solid lines; deconvoluted sub-bands: dots. (R^2 is always more than 0.99).

Table 2 Results of the deconvolution of the UV/vis spectra (Fig.3). Percentage of the sub-bands (I_1 at λ≈ 220 nm, I_2 at λ≈ 275 nm, I_3 at 300 < λ < 400 nm) and wt% Fe of the corresponding species.

Samples	I_1 *a (%)	Fe_1 (wt%)	I_2 *b (%)	Fe_2 (wt%)	I_3 *c (%)	Fe_3 (wt%)
Fe-0.17	73	0.125	24	0.04	3	0.005
Fe-0.27	68	0.18	25	0.07	7	0.02
Fe-0.52	58	0.30	28	0.15	14	0.07

*a isolated Fe^{3+} in tetrahedral coordination.

*b isolated Fe^{3+} in octahedral coordination.

*c oligomeric Fe_xO_y clusters.

EPR results

EPR spectra are also employed to study the nature and environment of different iron species, and EPR results for different samples are shown in Fig.4. Signals at $g \approx 4.3$ and $g \approx 6$ are frequently assigned to isolated Fe^{3+} in tetrahedral and distorted tetrahedral coordination[25-27], while signal at g ≈ 8.8 is assigned to isolated Fe^{3+} with a distorted octahedral environment [23]. Signal at g ≈ 2 is assigned to isolated Fe^{3+} in high-symmetry octahedral coordination or Fe_xO_y oligomers[23, 26, 28]. Furthermore, Pérez-Ramírez et al.[21] discussed the method to discriminate the two cases. The signal of isolated Fe^{3+} was narrow and the intensity increased with the decrease of temperature; however, the signal of Fe_xO_y oligomers was often broad and the temperature dependence was always different from paramagnetic behavior due to intrinsic antiferromagnetic interactions.

As shown in Fig.4, signals at g ≈ 4.3 and g ≈ 2 are observed in all samples and signals at g ≈ 6 and g ≈ 8.8 immerge with the increment of iron content. However, the contribution of various iron species to signal at g ≈ 2 is different. In Fe-0.17sample, signal at g ≈ 2 is narrow. According to the above analysis, it is caused by the isolated Fe^{3+} species. Furthermore, it is verified by the UV-vis result (seen in Fig.3), which suggests that only isolated Fe^{3+} exists in Fe-0.17sample. Since iron species in Fe-0.27 sample is dominated by isolated Fe^{3+} and small portion of Fe_xO_y oligomers, signal at g ≈ 2 in Fe-0.27 sample should be regarded as both isolated Fe^{3+} and Fe_xO_y oligomers. In Fe-0.52 sample, signal at g ≈ 2 tends to be broad and increases with the increment of temperature (seen in Fig. 4). Kumar et al.[20] found this was induced by the existence of the antiferromagnetically coupled Fe_xO_y species. So the g ≈ 2 signal in Fe-0.52 sample is due to Fe_xO_y oligomers.

In addition, the proportions of various iron species were also determined by a normalized double integration of the EPR spectra (Fig. 4)[23,29]. The relative percentage is listed in Table 3. The data demonstrates that the percentage of tetrahedral Fe^{3+} isolates decrease and the percentage of octahedral Fe^{3+} isolates increase with the increment of iron content, which is consistent with the trend derived from UV-vis result in Table 2.

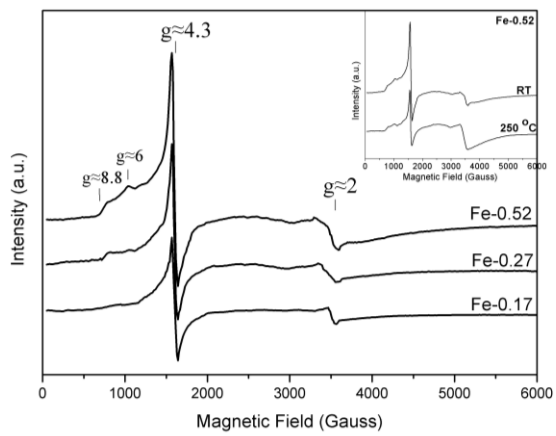

Fig.4. EPR spectra of Fe-beta samples recorded at room temperature after pre-oxidized at 550 ºC for 30 min and EPR spectra of Fe-0.52 sample at room temperature (RT) and 250 ºC.

Table 3 Percentage of various iron species derived from EPR spectra.

Samples	Fe_1*a (%)	Fe_2*b (%)	Fe_3*c (%)
Fe-0.17	78	22	0
Fe-0.27	66	23	11
Fe-0.52	60	27	13

*a isolated Fe^{3+} in tetrahedral coordination.

*b isolated Fe^{3+} in octahedral coordination.

*c oligomeric Fe_xO_y clusters.

3.3 The influence of iron species on NH_3-SCR activity

The UV-vis and EPR spectra illustrate that various iron species coexist in Fe-Beta samples and the NO_x conversion increases monotonically with the increment of iron loading during the test temperature range (see Fig. 1a). Hence we speculate that the various iron species play a different role in NH_3-SCR reaction. To investigate the contribution of different iron species in NH_3-SCR reaction, *in situ* EPR measurement was conducted. Since EPR is sensitive for Fe^{3+} species, *in situ* EPR is an effective method to study the variation of Fe^{3+} species and their role during the NH_3-SCR process at realistic temperatures.

Fig. 5 shows the *in situ* EPR spectra of Fe-Beta after exposure to the different gases. To well observe the changes of Fe^{3+} species, the catalyst was exposed to NH_3, NO and O_2 respectively[13, 19]. Considering that the Fe-0.52 sample has the richest Fe^{3+} species, it is elected to be the representative for this experiment. In addition, *in situ* EPR was recorded at 250 °C due to its best NH_3-SCR activity at low temperature in view of the requirement of equipment. Firstly, the Fe-0.52 sample was exposed to O_2 to make the catalyst active (see Fig. 5(1)). Comparing the spectra taken at room temperature (seen in Fig.4), the intensity of $g \approx 4.3$ signal decreases with rising temperature due to the Curie–Weiss law[30]. Secondly, the gas of NH_3 was passed through the catalyst, because NH_3 easily absorbed on the acid sites of the Fe-zeolite catalysts during the SCR reaction[1, 13]. The profile in Fig. 5(2) shows that the $g \approx 6$ and $g \approx 8.8$ signals almost disappear, while the $g \approx 4.3$ signal partly decreases. These signal changes suggest that the isolated Fe^{3+} is reduced to Fe^{2+} by NH_3. Furthermore, the isolated Fe^{3+} species in distorted tetrahedral and octahedral environment ($g \approx 6$ and $g \approx 8.8$) is more easily reducible than that in tetrahedral coordination ($g \approx 4.3$). The similar result was detected in Fe-ZSM-5 catalysts by Kumar et al[20, 31]. Thirdly, the gas of NO was cut in and NO reacted with the absorbed NH_3 and O species. Due to the consumption of NH_3, the intensity of EPR spectra ($g \geq 4.3$) is partly enhanced (see Fig. 5(3)). At last, the gas of O_2 was exposed to the catalyst again to re-oxidize the iron sites. Comparing the spectra of Fig. 5(4) with Fig. 5(1), it can be concluded that the signals at $g \approx 4.3$, 6 and 8.8, both the sites and intensity, are almost recovered. This finding illustrates that the reduced Fe^{2+} in Fig. 5(2) can be completely oxidized by the treatment of O_2. The profile changes from Fig. 6(1) to Fig. 5(4) well illustrate the dynamics of the isolated Fe^{3+} sites in Fe-Beta and its redox behavior during the NH_3-SCR process. It is reasonable to point out that the isolated Fe^{3+} species ($g \geq 4.3$) play a predominant role in NH_3-SCR reaction and isolated Fe^{3+} in different coordination present diverse reducibility. In contrast, the signal at $g \approx 2$ almost remains constant during the whole experiment; hence, Fe_xO_y oligomers exhibits weakly redox ability during the NH_3-SCR process.

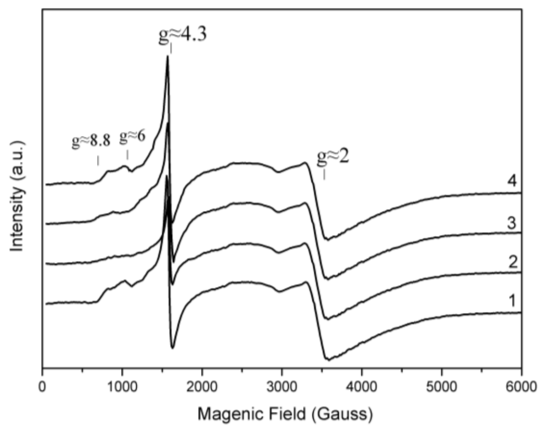

Fig.5. In situ EPR spectra of Fe-0.52 sample recorded at 250 ℃ during sequential treatment in a flow of (1) N_2 (pretreated in 5% O_2/N_2), (2) 0.1% NH_3/N_2 (3) 0.1% NO/N_2 and (4) 5% O_2/N_2. Each spectrum was measured after 1 h exposure time and under steady-state conditions.

In order to get a further understand the intrinsic effect of different iron species on the NH_3-SCR reaction, the kinetic experiments were performed over the Fe-Beta samples and the results are shown in Fig. 6. The NO_x conversion rates of the three samples indicate a similar order with the SCR activities in Fig.1a and the different rates are because of the number of active sites[32]. In addition, the parallel lines in Fig. 6 reveal that the catalysts have similar apparent activation energy (Ea= 40.6±1.5 kJ mol^{-1}) suggesting an identical rate controlling mechanism[33]. Compared with the most reported apparent Ea values (details with Table S1 are included in the supporting information), the apparent Ea value in this work is lower. The reason for that could be related to some intra-phase mass transfer limitations due to the pore structure[34] and/or the different gas adsorption behavior (such as NH_3, NO) [35]. Fig. 7 reveals the relationship between the amount of isolated Fe^{3+} species and turnover frequency (TOF). The result indicates that the TOF value of the three samples is almost constant at a certain temperature. This could prove that the isolated Fe^{3+} species are the active sites for NH_3-SCR reaction over Fe-Beta catalysts.

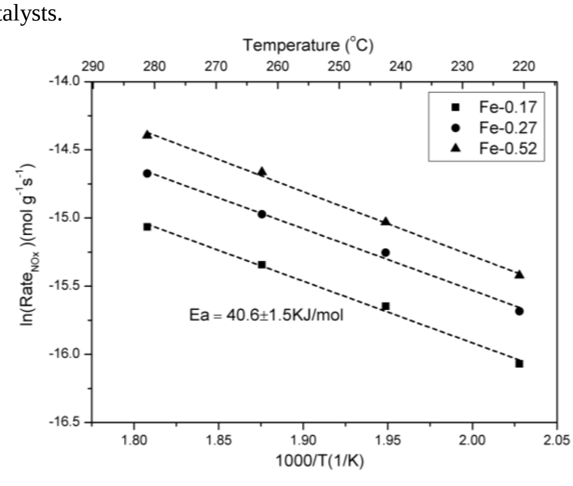

Fig.6. Arrhenius plots of the SCR reaction rates over Fe-Beta catalysts at 220 -280 °C. Conditions: 500 ppm NO, 500 ppmNH_3, 5% O_2, 8% CO_2, 5% H_2O balanced with N_2; flow rate: 1.5 L min^{-1}; GHSV: 420,000 h^{-1}.

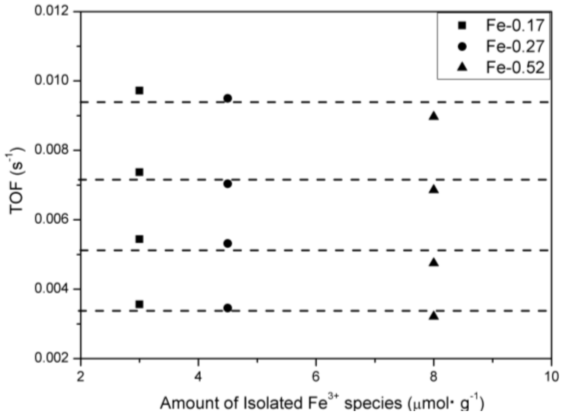

Fig. 7. Turnover frequency (TOF) for NH_3-SCR reaction with respect to the relative amount of isolated Fe^{3+} species over Fe-Beta catalysts. Conditions: 500 ppm NO, 500 ppmNH_3, 5% O_2, 8% CO_2, 5% H_2O balanced with N_2; flow rate: 1.5 L min^{-1}; GHSV: 420,000 h^{-1}.

3.4 The influence of iron species on NH_3 oxidation activity

Compared with the NH_3-SCR reaction, the effect of different iron species on NH_3 oxidation was also studied. Because the activity of NH_3 oxidation increase with the increment of oligomers (see Fig. 2 and Table 2), it is presumed oligomers are responsible for the oxidation of ammonia. In order to verify the inference, the kinetic experiments of NH_3 oxidation were performed. The results in Fig. 2 indicate that Fe-0.17 and H-Beta almost have the same activity of NH_3 oxidation. It is concluded that the acid sites perform NH_3 oxidation activity and the isolated Fe^{3+} in Fe-0.17 sample show inferior NH_3 oxidation activity. Hence, only Fe-0.27 and Fe-0.52 samples were elected to conduct the NH_3 oxidation kinetic experiment.

Fig. S5 (the supporting information) shows Arrhenius plots of the NH_3 oxidation rates over Fe-Beta catalysts at 460 °C -520 °C. The apparent activation energy (Ea) is almost constant for the two samples (Ea =110.4±3 kJ mol^{-1}). On the other hand, at each temperature the NH_3 oxidation rate increases monotonically with the increment of iron loading. Fig. S6 (the supporting information) reveals the relationship between the amount of oligomer species and turnover frequency (TOF). The result indicates that the TOF value of Fe-0.27 sample is a little higher than that of Fe-0.52 sample at the same temperature. Brandenberger et al[3] studied the relationship between iron species and NH_3 oxidation in Fe-ZSM-5 catalysts. They found that NH_3 oxidation was primarily carried out by lower clustered oligomers, or likely dimeric species. And the contribution of higher clustered oligomers became significant with rising temperature. For Fe-0.27 and Fe-0.52 samples, they not only have the different amount of oligomers, but they have the various clustered oligomers due to the different ion exchange level. Hence, it can be concluded that the difference of the TOF values between the two samples is because of the various clustered oligomers. And based on the above analysis, it is reasonable to conclude that the oligomer species are the active sites for NH_3 oxidation over Fe-Beta catalysts; moreover, the contribution of diverse clustered oligomers is unequal.

4. Conclusions

Three Fe-Beta catalysts with low iron loading (0.17-0.52 wt% Fe) were synthesized by liquid ion-exchange method. And diverse iron species exist in Fe-Beta. At iron content less than or equal to 0.17 wt%, the iron specie is almost only isolated Fe^{3+}. At higher Fe content (0.27-0.52 wt% Fe), the isolated Fe^{3+} in various coordination environment coexist with oligomers. The relationship between iron species and catalytic behavior in NH_3-SCR and NH_3 oxidation reaction was also investigated. *In situ* EPR spectra indicate that the isolated Fe^{3+} species in different coordination environment ($g \geq 4.3$) are very active in NH_3-SCR reaction. Furthermore, isolated Fe^{3+} species in distorted tetrahedral ($g \approx 6$) and octahedral ($g \approx 8.8$) environment present better reducibility than tetrahedral Fe^{3+} ($g \approx 4.3$). The results of kinetic experiments prove that isolated Fe^{3+} sites in diverse coordination environments are responsible for the active sites for NH_3-SCR reaction and oligomers are the active sites for NH_3 oxidation over Fe-Beta catalysts.

Acknowledgement

The authors are grateful to the financial support from the National High-Tech Research and Development Program of China (No. 2011AA03A405) and the Program of the Natural Science Foundation of China (No. 50972104).

Notes and references

[a] *Key Laboratory for Green Chemical Technology of State Education Ministry, School of Chemical Engineering & Technology, Tianjin University, Tianjin 300072, China. Tel./ Fax.: +86 22 27892301; E-mail: mqshen@tju.edu.cn*
[b] *State Key Laboratory of Engines, Tianjin University, Tianjin 300072, China*
[c] *Department of Chemistry, School of Science, Tianjin University of Commerce, Tianjin 300134, China*

1 M. Koebel, M. Elsener and M. Kleemann, *Catal. Today*, 2000, **59,** 335.
2 M. Schwidder, M. S. Kumar, K. Klementiev, M. M. Pohl, A. Brückner and W. Grünert, *J. Catal.*, 2005, **231**, 314.
3 S. Brandenberge, O. Kröcher, A. Tissler and R. Althoff, *Appl. Catal., B*, 2010, **95**, 348.
4 R. Q. Long and R. T. Yang, *J. Catal.*, 2002, **207,** 274.
5 M. Iwasaki, K. Yamazaki and H. Shinjoh, *Appl. Catal., B*, 2011, **102**, 302.
6 C. H. He, Y. H. Wang, Y. S. Cheng, C. K. Lambert and R. T. Yang, *Appl. Catal., A*, 2009, **368**, 121.
7 D. E. Doronkin, A. Y. Stakheev, A. V. Kucherov, N. N. Tolkachev, M. Kustova, M. Høj, G. N. Baeva, G. O. Bragina, P. Gabrielsson, I. Gekas and S. Dahl, *Top. Catal.*, 2009, **52,** 1728.
8 M. Høj, M. J. Beier, J. Grunwaldt and S. Dahl, *Appl. Catal., B*, 2009, **93,** 166.
9 L. Ma, H. Z. Chang, S. J. Yang, L. Chen, L. X. Fu and J. H. Li, *Chem. Eng. J.* 2012, **209,** 652.
10 A. M. Frey, S. Mert, J. Due-Hansen, R. Fehrmann and C. H. Christensen, *Catal Lett.*, 2009, **130,** 1.
11 P. Balle, B. Geiger and S. Kureti. *Appl. Catal., B*, 2009, **85,** 109.
12 A. V. Kucherov, D. E. Doronkin, A. Y. Stakheev, A. L. Kustov and M. Grill, *J. Mol. Catal. A: Chem.*, 2010, **325,** 73.
13 D. Klukowski, P. Balle, B. Geiger, S. Wagloehner, S. Kureti, B. Kimmerle, A. Baiker and J. D. Grunwaldt, *Appl. Catal., B*, 2009, **93,** 185.
14 M. Iwasaki and H. Shinjoh, *Chem. Commun.*, 2011, **47,** 3966.
15 S. M. Maier, A. Jentys, M. Janousch, J. A. V. Bokhoven and J. A. Lercher, *J. Phys. Chem. C*, 2012, ***116,*** 5846.
16 J. Kim, A. Jentys, S. M. Maier and J. A. Lercher, *J. Phys. Chem. C*, 2013,***117***, 986.

17 R. Nedyalkova, S. Shwan, M. Skoglundh and L. Olsson, *Appl. Catal., B*, 2013, **138,** 373.

18 S. Brandenberger, O. Kröcher, A. Tissler and R. Althoff, *Appl. Catal., A*, 2010, **373,** 168.

19 T. Ishihara, M. Kagawa, F. Hadama and Y. Takita , *J. Catal.*, 1997,**169,** 93,

20 M. S. Kumar, M. Schwidder, W. Grünert and A. Brückner, *J. Catal.*, 2004, **227,** 384.

21 J. Pérez-Ramírez, J.C. Groen, A. Brückner, M.S. Kumar, U. Bentrup, M. N. Debbagh and L.A. Villaescusa, *J. Catal.*, 2005, **232**, 318.

22 S. Bordiga, R. Buzzoni, F. Geobaldo, C. Lamberti, E. Giamello, A. Zecchina, G. Leofanti, G. Petrini, G. Tozzola and G. Vlaic, *J. Catal.*, 1996, **158,** 486.

23 E. A. Zhilinskaya, G. Delahay, M. Mauvezin, B. Coq, and A. Aboukaïs, *Langmuir* , 2003, **19,** 3596.

24 M. Mauvezin, G. Delahay, B. Coq, S. Kieger, J. C. Jumas and J. Olivier-Fourcade, *J. Phys. Chem. B*, 2001, **105,** 928.

25 T. Inui, H. Nagata, T. Takeguchi, S. Iwamoto, H. Matsuda and M. Inoue, *J. Catal.*, 1993, **139,** 482.

26 D. Goldfarb, M. Bernardo, K. G. Strohmaier, D. E. W. Vaughan and H. Thomann, *J. Am. Chem. Soc.*, 1994, **116,** 6344.

27 A. V. Kucherov and A. A. Slinkin, *Zeolites*, 1988, **8**,110.

28 S. Dzwigaj, L. Stievano, F. E. Wagner and M. Che, *J. Phys. Chem. Solids*, 2007, **68**, 1885.

29 A. V. Kucherov and M. Shelef, *J. Catal*., 2000, **195,** 106,

30 A.V. Kucherov, C.N. Montreuil, T.N. Kucherova and M. Shelef, *Catal Lett.*, 1998, **56,** 173.

31 M. S. Kumar, M. Schwidder, W. Grünert, U. Bentrup and A. Brückner, *J. Catal.*, 2006, **239**, 173.

32 K. Kamasamudram, N. W. Currier, X. Chen, A. Yezerets, *Catal. Today*, 2010, **151,** 212.

33 F. Gao, E. D. Walter, E. M. Karp, J. Luo, R. G. Tonkyn, J. Kwak, J. Szanyi and C. Peden. J. Catal., 2013, 300, 20,

34 J.M. Thomas and W.J. Thomas, *Principles and Practice of Heterogeneous Catalysis*, VCH, Weinheim, 1997.

35 B. Xu, C. Sievers, S.B. Hong, R. Prins, J.A. van Bokhoven, *J. Catal.*, 2006, **244,**163.